J. Appl. Comput. Mech., 8(4) (2022) 1343-1357
DOI: 10.22055/jacm.2022.39718.3452

ISSN: 2383-4536
jacm.scu.ac.ir

Shahid Chamran University of Ahvaz

Journal of Applied and Computational Mechanics

Research Paper

Dynamic Buckling of Stiffened Shell Structures with Transverse Shears under Linearly Increasing Load

Alexey Semenov

Department of Computer Science, Saint Petersburg State University of Architecture and Civil Engineering, 4, 2nd Krasnoarmeyskaya st., Saint-Petersburg, 190005, Russia

Received January 10 2022; Revised April 10 2022; Accepted for publication April 10 2022.
Corresponding author: A. Semenov (sw.semenov@gmail.com)

Abstract. Thin-walled shell structures are widely used in various fields of engineering, and the process of their deformation is essentially non-linear, which significantly complicates their analysis. The author presents a new mathematical model of shell structure deformation under dynamic loading, taking into account geometrical nonlinearity, transverse shears, and stiffeners. A distinctive feature of the model is the use of the refined discrete method to account for stiffeners, suggested by the author earlier. The method has previously been used only in static problems. It uses adjusting normalizing factors and makes it possible to obtain the most correct critical load values. A technique for numerically investigation of the process of deformation of such structures under dynamic loading is based on the L.V. Kantorovich method and Rosenbrock method for solution of a stiff ODE system. The proposed approach, in contrast to commercial software based on FEM, makes it possible to study in detail the supercritical deformation of structures, to identify patterns of influence of individual parts of the mathematical model on critical loads. Calculations for shallow doubly curved shells and cylindrical panels are provided. It is shown how the number of stiffeners affects the resulting buckling load values. A comparison with the classic discrete method to account for stiffeners is performed. Phase portraits of the system are given for all problems considered.

Keywords: Stiffened shell, buckling, refined model, phase portrait, dynamic load.

1. Introduction

Modeling the deformation of thin-walled shell structures is essential to solve numerous applied problems [1–3]. Depending on the properties of the structure material and types of external action, shells are studied using different mathematical models. Each such model represents a balance between the accuracy of the result and the computational complexity of the problem. Improved computing tools have made it possible to develop increasingly accurate models of shell structure deformation and obtain results of their analysis within an acceptable time.

One of the computationally complex problems is stress-strain state and buckling analysis in shell structures reinforced with a grid of stiffeners. Another complex problem is buckling analysis in shell structures under dynamic loading since, in buckling, the system of ordinary differential equations becomes stiff, and, to solve it, special numerical methods and significantly higher computing capacity are required. Many papers on the dynamics of shell structures describe studies of the vibration process and frequency analysis [4–27]. Meanwhile, buckling analysis has been studied less [20–33]. Azarboni, Ansari and Nazarinezhad [21] are numerically investigates the nonlinear chaotic and periodic dynamic responses of doubly curved shallow shells. The Galerkin method together with trigonometric mode shape functions is applied to solve the equations of motion. The critical values, phase portrait, Poincare maps, time history and power spectrum are presented to observe the behavior of the system. Lavrenčič and Brank [29] are studies shell buckling process by implicit structural dynamics time-stepping schemes with numerical dissipation. Computed numerical examples include classical shell buckling problems: snap-through, shell collapse, and buckling of perfect and imperfect cylinder under axial load. The dynamic results are compared with the static ones that were computed by the path-following method.

Many models are based on the Kirchhoff hypotheses (CSDT, "classic" models) [9–14, 33–35] where only three functions of normal displacements are unknown. A lot fewer papers use models based on the Timoshenko hypotheses (Reissner–Mindlin theory, FSDT) [6, 18, 21] where another two functions of normal rotation angles are added to the unknown functions of displacements. This model is more accurate since it takes into account transverse shears, which is especially important in the analysis of shells reinforced with stiffeners. In [18], the behavior of a circular elastoplastic structure, consisting of a shell and reinforced ribs, under the action of dynamic loads, has been investigated. The relationship between deformations and displacements is taken geometrically nonlinear. The solution of the differential equations for the vibrations of the structure, taking into account the elastoplastic properties of the shell materials and the reinforced ribs, is carried out by the finite difference method. The works [3, 11–20, 32–37] address the analysis of stiffened structures, of which papers [11–18, 34–36] use the discrete method to account for stiffeners (in various modifications). This approach is the most accurate. However, it is computationally consuming.

Published online: April 21 2022

Huang and Qiao [36] are studies nonlinear buckling of rotationally-restrained stiffened laminated composite doubly-curved shallow shells with imperfection subjected to in-plane shear and compression loading. The new equivalent model with variable stiffness for both centrically- and eccentrically-stiffened shells is developed, and Heaviside function is uniquely applied to construct the variable stiffness of stiffened shells along two orthogonal directions.

The application of mathematical models in a mixed form (where the function of vertical displacements and the stress function are used) is shown in [21–24, 26, 30, 36]. In terms of the load direction, the axial load is studied most often [20, 23–25, 35, 38], while the load distributed over the surface is studied less often [20, 23, 30, 39–41]. Periodic impacts are considered in [8, 21, 24].

It is also worth noting papers that present results of experimental studies of shell structures [17, 32, 37, 42]. In [32] dynamic buckling of grid-stiffened cylindrical shells submerged in a large opening pond at a depth of 5 m and subjected to radial intermediate-velocity impact was experimentally investigated. Measurements of hoop and axial strains reveal that global buckling of skin and stiffeners of the grid-stiffened cylindrical shell occurred under bubble pulsation loads, which features mutation and separation of strains and a sudden change in the vibration period of the stiffened shell with a small increment of impulse. Ghasemi et al. [37] shows that the application of their novel optimization algorithm leads to a decrease of 21 % and 28 % in optimum local mass of stiffened unsymmetrical angle-ply and unstiffened symmetrical angle-ply laminated composite shells, respectively.

Significant modern research is related to the optimization and design of structures with variable stiffness [43, 44]. In [43] an integrated framework of exact modeling, isogeometric analysis and optimization for variable stiffness composite panels is established, aiming to improve the solution accuracy, efficiency and facilitate the design optimization, and a novel multi-start gradient-based strategy is developed to enhance global optimization capacity. In [44], a novel layout optimization method is proposed for curvilinearly stiffened panels based on deep learning-based models, which enables their intelligent design. Unlike traditional methods, the image-based structural layout, which is characteristic of curvilinear stiffener paths, is employed as a design variable, and convolutional neural networks (CNNs) are used to extract the layout features from the curvilinear stiffeners and construct a surrogate model between layout features and structural performance.

The objective of the study was to present a new mathematical model of shell structure deformation under dynamic loading, taking into account geometrical nonlinearity, transverse shears, and stiffeners. A distinctive feature of the model is the use of the refined discrete method to account for stiffeners, suggested by the author earlier in [45]. The method has previously been used only in static problems [46]. In this paper, only orthogonal grids of stiffeners, consisting of rectangular cross-section ribs, are considered, however, these results can become the basis for further studies of other options for stiffening the structure.

2. Theory and Methods

2.1 Governing equations

The stiffened shell structures of an arbitrary kind with skin thickness h are considered, taking into account geometric nonlinearity, lateral shifts and inertia of rotation. The middle surface of the shell is taken as a coordinate surface. Axes x and y are directed along the main shell curvature lines, and axis z along the normal to the middle surface in the direction of the concavity (Fig. 1).

It will be considered a shell deformation model of the Timoshenko type (Mindlin–Reissner), and displacements in the layer at distance z from the middle surface will be:

$$U^z = U + z\Psi_x, \quad V^z = V + z\Psi_y, \quad W^z = W. \tag{1}$$

Here $U = U(x,y,t)$, $V = V(x,y,t)$, $W = W(x,y,t)$ are unknown functions of displacements, and $\Psi_x = \Psi_x(x,y,t)$, $\Psi_y = \Psi_y(x,y,t)$ are unknown functions of the rotation angles of the normal in the planes xOz and yOz, respectively. In this case, taking into account geometrical nonlinearity and transverse shears, the geometric relationships in the middle surface of the shell will have the form:

$$\begin{gathered}
\varepsilon_x = \frac{1}{A}\frac{\partial U}{\partial x} + \frac{1}{AB}V\frac{\partial A}{\partial y} - k_x W + \frac{1}{2}\theta_1^2, \quad \varepsilon_y = \frac{1}{B}\frac{\partial V}{\partial y} + \frac{1}{AB}U\frac{\partial B}{\partial x} - k_y W + \frac{1}{2}\theta_2^2, \quad \gamma_{xy} = \frac{1}{A}\frac{\partial V}{\partial x} + \frac{1}{B}\frac{\partial U}{\partial y} - \frac{1}{AB}U\frac{\partial A}{\partial y} - \frac{1}{AB}V\frac{\partial B}{\partial x} + \theta_1\theta_2, \\
\theta_1 = -\left(\frac{1}{A}\frac{\partial W}{\partial x} + k_x U\right), \quad \theta_2 = -\left(\frac{1}{B}\frac{\partial W}{\partial y} + k_y V\right), \quad k_x = \frac{1}{R_1}, \quad k_y = \frac{1}{R_2}, \\
\chi_1 = \frac{1}{A}\frac{\partial \Psi_x}{\partial x} + \frac{1}{AB}\frac{\partial A}{\partial y}\Psi_y, \quad \chi_2 = \frac{1}{B}\frac{\partial \Psi_y}{\partial y} + \frac{1}{AB}\frac{\partial B}{\partial x}\Psi_x, \quad \chi_{12} = \frac{1}{2}\left(\frac{1}{A}\frac{\partial \Psi_y}{\partial x} + \frac{1}{B}\frac{\partial \Psi_x}{\partial y} - \frac{1}{AB}\frac{\partial B}{\partial x}\Psi_y - \frac{1}{AB}\frac{\partial A}{\partial y}\Psi_x\right),
\end{gathered} \tag{2}$$

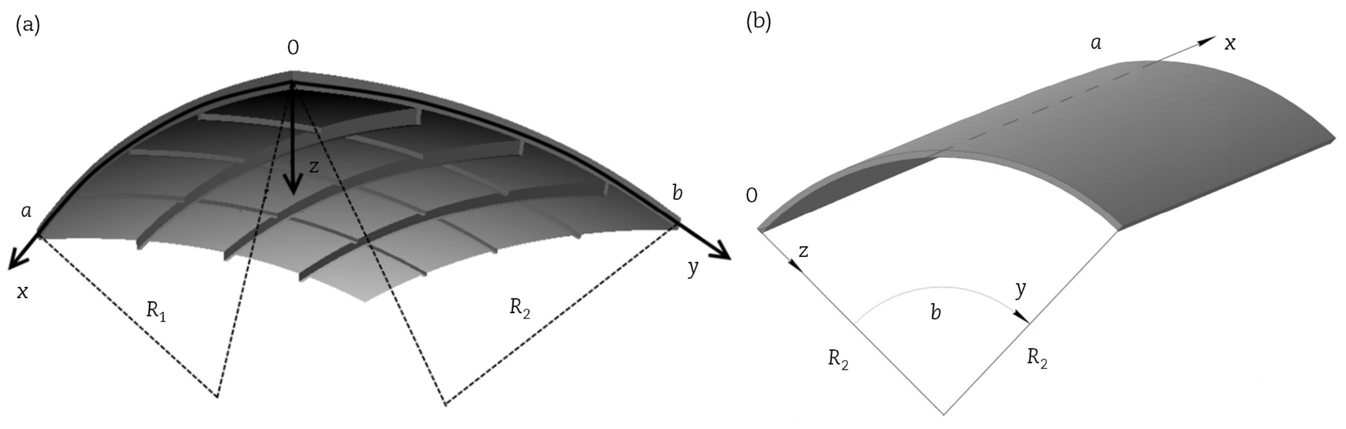

Fig. 1. Layout view of the shells

Table 1. Values of Lamé parameters and curvatures for some types of shells

	A	B	R_1	R_2
Doubly-curved shallow shell	1	1	const.	const.
Cylindrical shell	1	R_2	∞	const.
Conical shell	1	$x\cdot\sin\theta$	∞	$x\cdot tg\theta$
Spherical shell	R	$R\cdot\sin x$	R	R
Toroidal shell	R	$d_1+R\cdot\sin x$	R	$[d_1+R\cdot\sin x]/\sin x$

where $\varepsilon_x,\varepsilon_y$ are the axial strain along the x, y coordinates of the middle surface; $\gamma_{xy},\gamma_{xz},\gamma_{yz}$ are the shear strain in the xOy, xOz, yOz planes, respectively; χ_1,χ_2,χ_{12} are functions of the change of curvature and torsion; A,B are Lamé parameters (Table 1); k_x,k_y are the primary curvatures of the shell along the x and y axes; R_1,R_2 are the principal curvature radii characterizing the geometry of the shell; $f(z)$ is a function characterizing the distribution of shear strains γ_{xz},γ_{yz} along the thickness of the shell; and $k=5/6$ is a numerical coefficient.

Physical relationships for linearly elastic deformation of isotropic materials in a plane stress state will have the form:

$$\sigma_x=\frac{E}{1-\mu^2}\left[\varepsilon_x+\mu\varepsilon_y+z(\chi_1+\mu\chi_2)\right],\quad \sigma_y=\frac{E}{1-\mu^2}\left[\varepsilon_y+\mu\varepsilon_x+z(\chi_2+\mu\chi_1)\right],$$
$$\tau_{xy}=\frac{E}{2(1+\mu)}\left[\gamma_{xy}+2z\chi_{12}\right],\quad \tau_{xz}=\frac{E}{2(1+\mu)}\gamma_{xz},\quad \tau_{yz}=\frac{E}{2(1+\mu)}\gamma_{yz}. \tag{3}$$

Here E, μ are the elastic moduli and Poisson coefficient of the shell material.

Despite the fact that the shell material is isotropic, it can deform asymmetrically in the case of a different number of stiffeners, the choice of different geometric shapes, or under a non-uniform applied load.

Total deformation energy of a shell structure can be written using the functional [47]:

$$I=\int_{t_0}^{t_1}(E_k-E_s)dt, \tag{4}$$

where E_k is the kinetic deformation energy of the system; and $E_s=E_p-A$ is the functional of a static problem equal to the difference in the potential deformation energy of the system and the work of external forces. For stiffened shells, the potential and kinetic energy as the sum of the skin energy (superscript "0") and the energy of the stiffeners (superscript "R") are represents

$$E_p=E_p^0+E_p^R,\quad E_k=E_k^0+E_k^R. \tag{5a}$$

Thus,

$$I=\int_{t_0}^{t_1}\left(E_k^0+E_k^R-E_p^0-E_p^R+A\right)dt,$$

$$E_k^0=\frac{\rho}{2}\int_{a_1}^{a}\int_{0}^{b}\left\{h\left[\left(\frac{\partial U}{\partial t}\right)^2+\left(\frac{\partial V}{\partial t}\right)^2+\left(\frac{\partial W}{\partial t}\right)^2\right]+\frac{h^3}{12}\left[\left(\frac{\partial\Psi_x}{\partial t}\right)^2+\left(\frac{\partial\Psi_y}{\partial t}\right)^2\right]\right\}ABdxdy,$$

$$E_k^R=\frac{\rho}{2}\int_{a_1}^{a}\int_{0}^{b}\left\{\bar{F}_p\left[\left(\frac{\partial U}{\partial t}\right)^2+\left(\frac{\partial V}{\partial t}\right)^2+\left(\frac{\partial W}{\partial t}\right)^2\right]+2\bar{S}_p\left[\frac{\partial U}{\partial t}\frac{\partial\Psi_x}{\partial t}+\frac{\partial V}{\partial t}\frac{\partial\Psi_y}{\partial t}\right]+\bar{J}_p\left[\left(\frac{\partial\Psi_x}{\partial t}\right)^2+\left(\frac{\partial\Psi_y}{\partial t}\right)^2\right]\right\}ABdxdy, \tag{5b}$$

$$E_p^0=\frac{1}{2}\int_{a_1}^{a}\int_{0}^{b}\left(N_x^0\varepsilon_x+N_y^0\varepsilon_y+\frac{1}{2}\left(N_{xy}^0+N_{yx}^0\right)\gamma_{xy}+M_x^0\chi_1+M_y^0\chi_2+\left(M_{xy}^0+M_{yx}^0\right)\chi_{12}+Q_x^0(\Psi_x-\theta_1)+Q_y^0(\Psi_y-\theta_2)\right)ABdxdy,$$

$$E_p^R=\frac{1}{2}\int_{a_1}^{a}\int_{0}^{b}\left(N_x^R\varepsilon_x+N_y^R\varepsilon_y+\frac{1}{2}\left(N_{xy}^R+N_{yx}^R\right)\gamma_{xy}+M_x^R\chi_1+M_y^R\chi_2+\left(M_{xy}^R+M_{yx}^R\right)\chi_{12}+Q_x^R(\Psi_x-\theta_1)+Q_y^R(\Psi_y-\theta_2)\right)ABdxdy,$$

$$A=\frac{1}{2}\int_{a_1}^{a}\int_{0}^{b}\left(2qW+2P_xU+2P_yV\right)ABdxdy\ ,$$

where q, P_x, P_y denote load components; ρ – density of the material; $\bar{F}_p,\bar{S}_p,\bar{J}_p$ – parameters of stiffeners (will be described later); N_x,N_y denote normal forces in the direction of the x,y coordinates; N_{xy},N_{yx} denote shear forces in the corresponding plane xOy; M_x,M_y denote bending moments; M_{xy},M_{yx} denote torque moments; Q_x,Q_y denote transverse forces in the planes xOz and yOz, which are defined by the following relationships for the structural skin (superscript 0):

$$N_x^0=\frac{Eh}{1-\mu^2}\left(\varepsilon_x+\mu\varepsilon_y\right),\quad N_y^0=\frac{Eh}{1-\mu^2}\left(\varepsilon_y+\mu\varepsilon_x\right),\quad M_x^0=\frac{Eh^3}{12\left(1-\mu^2\right)}(\chi_1+\mu\chi_2),\quad M_y^0=\frac{Eh^3}{12\left(1-\mu^2\right)}(\chi_2+\mu\chi_1),$$
$$N_{xy}^0=N_{yx}^0=\frac{E}{2(1+\mu)}h\gamma_{xy},\quad M_{xy}^0=M_{yx}^0=\frac{Eh^3}{12(1+\mu)}\chi_{12},\quad Q_x^0=\frac{E}{2(1+\mu)}kh(\Psi_x-\theta_1),\quad Q_y^0=\frac{E}{2(1+\mu)}kh\left(\Psi_y-\theta_2\right). \tag{6}$$

In the case of non-uniform lateral load, it is necessary to specified as follows:

$$q = q_0\left(a_{11} + a_{21}x + a_{31}x^2\right)\left(a_{12} + a_{22}y + a_{32}y^2\right) + q_{sv},$$

where q_0 denotes the value of the transverse load, MPa; q_{sv} denotes the own weight of the shell, MPa; a_{ij} – coefficients that allows to set the shape of the distribution of the applied load. For example, for a linearly increasing load, it will be $a_{11} = -a_1/(a-a_1), a_{21} = 1/(a-a_1), a_{31} = 0$, $a_{12} = 0, a_{22} = 1/b, a_{32} = 0$ and for an evenly distributed load, it will be $a_{11} = 1, a_{21} = 0, a_{31} = 0$, $a_{12} = 1, a_{22} = 0, a_{32} = 0$.

2.2 Refined model of stiffeners

The discrete layer of shell stiffeners is described by the function $H(x,y)$, which characterizes the height and location of the stiffeners with regard to the shell:

$$H(x,y) = \sum_{j=1}^{m} h^j \bar{\delta}\left(x - x_j\right) + \sum_{i=1}^{n} h^i \bar{\delta}\left(y - y_i\right) - \sum_{i=1}^{n}\sum_{j=1}^{m} h^{ij} \bar{\delta}\left(x - x_j\right)\bar{\delta}\left(y - y_i\right), \tag{7}$$

where h^i, h^j are the height of stiffeners; i and j indicate stiffeners parallel to the x and y axes, respectively; n, m are the number of stiffeners; $h^{ij} = \min\left\{h^i, h^j\right\}$, i.e. the common portion of intersecting stiffeners; $\bar{\delta}\left(x - x_j\right)$ and $\bar{\delta}\left(y - y_i\right)$ are unit column functions representing the differences between unit functions $\bar{\delta}\left(x - x_j\right) = U\left(x - a_j\right) - U\left(x - b_j\right)$; $\bar{\delta}\left(y - y_i\right) = U\left(y - c_i\right) - U\left(y - d_i\right)$, where $a_j = x_j - r_j/(2A)$, $b_j = x_j + r_j/(2A)$, $c_i = y_i - r_i/(2B)$, $d_i = y_i + r_i/(2B)$ (width of stiffeners r_i, r_j is given in meters for any rotational shells).

Since the Lame parameter A is constant for rotational shells, and the Lame parameter B equals $B(x)$, then a_j, b_j, are constants. To ensure the same width of the i^{th} stiffeners at any x, $c_i = c_i(x), d_i = d_i(x)$.

If the location of the stiffeners is defined in such manner, the contact between the skin and stiffeners will be along a strip. Where they intersect, stiffeners are rigidly fixed against each other. Therefore, the thickness of the entire structure equals $h + H$, where h is the thickness of the skin.

Therefore, the forces and moments acting in stiffeners will be as follows:

$$\begin{gathered}
N_x^R = \frac{E}{1-\mu^2}\left(\bar{F}_x\left(\varepsilon_x + \mu\varepsilon_y\right) + \bar{S}_x\left(\chi_1 + \mu\chi_2\right)\right), \quad M_x^R = \frac{E}{1-\mu^2}\left[\bar{S}_x\left(\varepsilon_x + \mu\varepsilon_y\right) + \bar{J}_x\left(\chi_1 + \mu\chi_2\right)\right], \\
N_y^R = \frac{E}{1-\mu^2}\left[\bar{F}_y\left(\varepsilon_y + \mu\varepsilon_x\right) + \bar{S}_y\left(\chi_2 + \mu\chi_1\right)\right], \quad M_y^R = \frac{E}{1-\mu^2}\left[\bar{S}_y\left(\varepsilon_y + \mu\varepsilon_x\right) + \bar{J}_y\left(\chi_2 + \mu\chi_1\right)\right], \\
N_{xy}^R = N_{yx}^R = \frac{E}{2(1+\mu)}\left[\bar{F}_{xy}\gamma_{xy} + 2\bar{S}_{xy}\chi_{12}\right], \quad M_{xy}^R = M_{yx}^R = \frac{E}{2(1+\mu)}\left[\bar{S}_{xy}\gamma_{xy} + \bar{J}_{xy}\chi_{12}\right], \\
Q_x^R = \frac{E}{2(1+\mu)}k\bar{F}_x\left(\Psi_x - \theta_1\right), \quad Q_y^R = \frac{E}{2(1+\mu)}k\bar{F}_y\left(\Psi_y - \theta_2\right).
\end{gathered} \tag{8}$$

Author suggested introducing the modular ratio for stiffness properties when shells are discretely reinforced with stiffeners.

The total stiffness includes that of stiffeners in the direction under consideration and that of stiffeners in the orthogonal direction.

$$\begin{gathered}
\bar{F}_x = \sum_{i=1}^{n} F^i \bar{\delta}\left(y - y_i\right) + r_a\left[\sum_{j=1}^{m} F^j \bar{\delta}\left(x - x_j\right) - \sum_{i=1}^{n}\sum_{j=1}^{m} F^{ij}\bar{\delta}\left(x - x_j\right)\bar{\delta}\left(y - y_i\right)\right], \\
\bar{S}_x = \sum_{i=1}^{n} S^i \bar{\delta}\left(y - y_i\right) + r_a\left[\sum_{j=1}^{m} S^j \bar{\delta}\left(x - x_j\right) - \sum_{i=1}^{n}\sum_{j=1}^{m} S^{ij}\bar{\delta}\left(x - x_j\right)\bar{\delta}\left(y - y_i\right)\right], \\
\bar{J}_x = \sum_{i=1}^{n} J^i \bar{\delta}\left(y - y_i\right) + r_a\left[\sum_{j=1}^{m} J^j \bar{\delta}\left(x - x_j\right) - \sum_{i=1}^{n}\sum_{j=1}^{m} J^{ij}\bar{\delta}\left(x - x_j\right)\bar{\delta}\left(y - y_i\right)\right], \\
\bar{F}_y = \sum_{j=1}^{m} F^j \bar{\delta}\left(x - x_j\right) + r_b\left[\sum_{i=1}^{n} F^i \bar{\delta}\left(y - y_i\right) - \sum_{i=1}^{n}\sum_{j=1}^{m} F^{ij}\bar{\delta}\left(x - x_j\right)\bar{\delta}\left(y - y_i\right)\right], \\
\bar{S}_y = \sum_{j=1}^{m} S^j \bar{\delta}\left(x - x_j\right) + r_b\left[\sum_{i=1}^{n} S^i \bar{\delta}\left(y - y_i\right) - \sum_{i=1}^{n}\sum_{j=1}^{m} S^{ij}\bar{\delta}\left(x - x_j\right)\bar{\delta}\left(y - y_i\right)\right], \\
\bar{J}_y = \sum_{j=1}^{m} J^j \bar{\delta}\left(x - x_j\right) + r_b\left[\sum_{i=1}^{n} J^i \bar{\delta}\left(y - y_i\right) - \sum_{i=1}^{n}\sum_{j=1}^{m} J^{ij}\bar{\delta}\left(x - x_j\right)\bar{\delta}\left(y - y_i\right)\right], \\
\bar{F}_{xy} = \frac{1}{2}\left(\bar{F}_x + \bar{F}_y\right) = \frac{1}{2}\sum_{i=1}^{n} F^i\left(1 + r_b\right)\bar{\delta}\left(y - y_i\right) + \frac{1}{2}\sum_{j=1}^{m} F^j\left(1 + r_a\right)\bar{\delta}\left(x - x_j\right) - \sum_{i=1}^{n}\sum_{j=1}^{m} F^{ij} r_{ab}\bar{\delta}\left(x - x_j\right)\bar{\delta}\left(y - y_i\right), \\
\bar{S}_{xy} = \frac{1}{2}\left(\bar{S}_x + \bar{S}_y\right) = \frac{1}{2}\sum_{i=1}^{n} S^i\left(1 + r_b\right)\bar{\delta}\left(y - y_i\right) + \frac{1}{2}\sum_{j=1}^{m} S^j\left(1 + r_a\right)\bar{\delta}\left(x - x_j\right) - \sum_{i=1}^{n}\sum_{j=1}^{m} S^{ij} r_{ab}\bar{\delta}\left(x - x_j\right)\bar{\delta}\left(y - y_i\right), \\
\bar{J}_{xy} = \frac{1}{2}\left(\bar{J}_x + \bar{J}_y\right) = \frac{1}{2}\sum_{i=1}^{n} J^i\left(1 + r_b\right)\bar{\delta}\left(y - y_i\right) + \frac{1}{2}\sum_{j=1}^{m} J^j\left(1 + r_a\right)\bar{\delta}\left(x - x_j\right) - \sum_{i=1}^{n}\sum_{j=1}^{m} J^{ij} r_{ab}\bar{\delta}\left(x - x_j\right)\bar{\delta}\left(y - y_i\right),
\end{gathered} \tag{9}$$

where,

$$F^i = h^i,\quad F^j = h^j,\quad F^{ij} = h^{ij},\quad S^i = \frac{h^i\left(h+h^i\right)}{2},\quad S^j = \frac{h^j\left(h+h^j\right)}{2},\quad S^{ij} = \frac{h^{ij}\left(h+h^{ij}\right)}{2},$$
$$J^i = 0.25h^2h^i + 0.5h\left(h^i\right)^2 + \frac{1}{3}\left(h^i\right)^3,\quad J^j = 0.25h^2h^j + 0.5h\left(h^j\right)^2 + \frac{1}{3}\left(h^j\right)^3,\quad J^{ij} = 0.25h^2h^{ij} + 0.5h\left(h^{ij}\right)^2 + \frac{1}{3}\left(h^{ij}\right)^3 \tag{10}$$

and

$$r_a = \frac{r_j}{aA},\quad r_b = \frac{r_i}{bB},\quad r_{ab} = \frac{r_a + r_b}{2}. \tag{11}$$

Besides, in contrast to static problems, it is suggested to introduce stiffness characteristics without using adjusting factors when determining kinetic energy in dynamic problems:

$$\bar{F}_p = \sum_{i=1}^{n} F^i\bar{\delta}\left(y-y_i\right) + \sum_{j=1}^{m} F^j\bar{\delta}\left(x-x_j\right) - \sum_{i=1}^{n}\sum_{j=1}^{m} F^{ij}\bar{\delta}\left(x-x_j\right)\bar{\delta}\left(y-y_i\right),$$
$$\bar{S}_p = \sum_{i=1}^{n} S^i\bar{\delta}\left(y-y_i\right) + \sum_{j=1}^{m} S^j\bar{\delta}\left(x-x_j\right) - \sum_{i=1}^{n}\sum_{j=1}^{m} S^{ij}\bar{\delta}\left(x-x_j\right)\bar{\delta}\left(y-y_i\right), \tag{12}$$
$$\bar{J}_p = \sum_{i=1}^{n} J^i\bar{\delta}\left(y-y_i\right) + \sum_{j=1}^{m} J^j\bar{\delta}\left(x-x_j\right) - \sum_{i=1}^{n}\sum_{j=1}^{m} J^{ij}\bar{\delta}\left(x-x_j\right)\bar{\delta}\left(y-y_i\right).$$

To calculate integrals of columnar functions in expressions for E_k^R, E_s^R, the following transformations are performed. The double integral is converted into iterated integrals, and then Simpson's rule is applied. The integral with respect to x is the outer integral, because, at each value of x, the integral with respect to y is calculated first, as it includes a member that depends on x $(r_b = r_i/[bB(x)])$. When the equations of forces and moments are applied to (5), this will lead to:

$$E_p^R = \frac{1}{2}\int_{a_1}^{a}\int_{0}^{b}\left[\sum_{j=1}^{m} A_1^j\bar{\delta}\left(x-x_j\right) + \sum_{i=1}^{n} A_2^i\bar{\delta}\left(y-y_i\right) - \sum_{i=1}^{n}\sum_{j=1}^{m} A_3^{ij}\bar{\delta}\left(x-x_j\right)\bar{\delta}\left(y-y_i\right)\right]dxdy,$$
$$E_k^R = \frac{\rho}{2}\int_{a_1}^{a}\int_{0}^{b}\left[\sum_{j=1}^{m} A_4^j\bar{\delta}\left(x-x_j\right) + \sum_{i=1}^{n} A_5^i\bar{\delta}\left(y-y_i\right) - \sum_{i=1}^{n}\sum_{j=1}^{m} A_6^{ij}\bar{\delta}\left(x-x_j\right)\bar{\delta}\left(y-y_i\right)\right]dxdy. \tag{13}$$

Here,

$$A_1^j = \left[\frac{E}{1-\mu^2}\left(F^j\left(\varepsilon_x + \mu\varepsilon_y\right)\varepsilon_x + S^j\left(\chi_1 + \mu\chi_2\right)\varepsilon_x\right)r_a + \frac{E}{1-\mu^2}\left(F^j\left(\varepsilon_y + \mu\varepsilon_x\right)\varepsilon_y + S^j\left(\chi_2 + \mu\chi_1\right)\varepsilon_y\right) + \frac{1}{2}\frac{E}{2(1+\mu)}\left(F^j\gamma_{xy}^2 + 2S^j\chi_{12}\gamma_{xy}\right)(1+r_a) + \right.$$
$$+\frac{E}{1-\mu^2}\left(S^j\left(\varepsilon_x + \mu\varepsilon_y\right)\chi_1 + J^j\left(\chi_1 + \mu\chi_2\right)\chi_1\right)r_a + \frac{E}{1-\mu^2}\left(S^j\left(\varepsilon_y + \mu\varepsilon_x\right)\chi_2 + J^j\left(\chi_2 + \mu\chi_1\right)\chi_2\right) + \frac{E}{2(1+\mu)}\left(S^j\gamma_{xy}\chi_{12} + 2J^j\chi_{12}^2\right)(1+r_a) +$$
$$\left. + \frac{E}{2(1+\mu)}k\left(\Psi_x - \theta_1\right)^2 F^j r_a + \frac{E}{2(1+\mu)}k\left(\Psi_y - \theta_2\right)^2 F^j\right]AB,$$

$$A_2^i = \left[\frac{E}{1-\mu^2}\left(F^i\left(\varepsilon_x + \mu\varepsilon_y\right)\varepsilon_x + S^i\left(\chi_1 + \mu\chi_2\right)\varepsilon_x\right) + \frac{E}{1-\mu^2}\left(F^i\left(\varepsilon_y + \mu\varepsilon_x\right)\varepsilon_y + S^i\left(\chi_2 + \mu\chi_1\right)\varepsilon_y\right)r_b + \frac{1}{2}\frac{E}{2(1+\mu)}\left(F^i\gamma_{xy}^2 + 2S^i\chi_{12}\gamma_{xy}\right)(1+r_b) + \right.$$
$$+\frac{E}{1-\mu^2}\left(S^i\left(\varepsilon_x + \mu\varepsilon_y\right)\chi_1 + J^i\left(\chi_1 + \mu\chi_2\right)\chi_1\right) + \frac{E}{1-\mu^2}\left(S^i\left(\varepsilon_y + \mu\varepsilon_x\right)\chi_2 + J^i\left(\chi_2 + \mu\chi_1\right)\chi_2\right)r_b + \frac{E}{2(1+\mu)}\left(S^i\gamma_{xy}\chi_{12} + 2J^i\chi_{12}^2\right)(1+r_b) +$$
$$\left. + \frac{E}{2(1+\mu)}k\left(\Psi_x - \theta_1\right)^2 F^i + \frac{E}{2(1+\mu)}k\left(\Psi_y - \theta_2\right)^2 F^i r_b\right]AB,$$

$$A_3^{ij} = \left[\frac{E}{1-\mu^2}\left(F^{ij}\left(\varepsilon_x + \mu\varepsilon_y\right)\varepsilon_x + S^{ij}\left(\chi_1 + \mu\chi_2\right)\varepsilon_x\right)r_a + \frac{E}{1-\mu^2}\left(F^{ij}\left(\varepsilon_y + \mu\varepsilon_x\right)\varepsilon_y + S^{ij}\left(\chi_2 + \mu\chi_1\right)\varepsilon_y\right)r_b + \frac{E}{2(1+\mu)}\left(F^{ij}\gamma_{xy}^2 + 2S^{ij}\chi_{12}\gamma_{xy}\right)r_{ab} + \right.$$
$$+\frac{E}{1-\mu^2}\left(S^{ij}\left(\varepsilon_x + \mu\varepsilon_y\right)\chi_1 + J^{ij}\left(\chi_1 + \mu\chi_2\right)\chi_1\right)r_a + \frac{E}{1-\mu^2}\left(S^{ij}\left(\varepsilon_y + \mu\varepsilon_x\right)\chi_2 + J^{ij}\left(\chi_2 + \mu\chi_1\right)\chi_2\right)r_b + 2\frac{E}{2(1+\mu)}\left(S^{ij}\gamma_{xy}\chi_{12} + 2J^{ij}\chi_{12}^2\right)r_{ab} + \tag{14}$$
$$\left. + \frac{E}{2(1+\mu)}k\left(\Psi_x - \theta_1\right)^2 F^{ij} r_a + \frac{E}{2(1+\mu)}k\left(\Psi_y - \theta_2\right)^2 F^{ij} r_b\right]AB,$$

$$A_4^j = \left(F^j\left[\left(\frac{\partial U}{\partial t}\right)^2 + \left(\frac{\partial V}{\partial t}\right)^2 + \left(\frac{\partial W}{\partial t}\right)^2\right] + 2S^j\left[\frac{\partial U}{\partial t}\frac{\partial \Psi_x}{\partial t} + \frac{\partial V}{\partial t}\frac{\partial \Psi_y}{\partial t}\right] + J^j\left[\left(\frac{\partial \Psi_x}{\partial t}\right)^2 + \left(\frac{\partial \Psi_y}{\partial t}\right)^2\right]\right)AB,$$
$$A_5^i = \left(F^i\left[\left(\frac{\partial U}{\partial t}\right)^2 + \left(\frac{\partial V}{\partial t}\right)^2 + \left(\frac{\partial W}{\partial t}\right)^2\right] + 2S^i\left[\frac{\partial U}{\partial t}\frac{\partial \Psi_x}{\partial t} + \frac{\partial V}{\partial t}\frac{\partial \Psi_y}{\partial t}\right] + J^i\left[\left(\frac{\partial \Psi_x}{\partial t}\right)^2 + \left(\frac{\partial \Psi_y}{\partial t}\right)^2\right]\right)AB,$$
$$A_6^{ij} = \left(F^{ij}\left[\left(\frac{\partial U}{\partial t}\right)^2 + \left(\frac{\partial V}{\partial t}\right)^2 + \left(\frac{\partial W}{\partial t}\right)^2\right] + 2S^{ij}\left[\frac{\partial U}{\partial t}\frac{\partial \Psi_x}{\partial t} + \frac{\partial V}{\partial t}\frac{\partial \Psi_y}{\partial t}\right] + J^{ij}\left[\left(\frac{\partial \Psi_x}{\partial t}\right)^2 + \left(\frac{\partial \Psi_y}{\partial t}\right)^2\right]\right)AB.$$

Functional (13) can be written as follows:

$$E_p^R = \frac{1}{2}\left(\int_0^b dy \sum_{j=1}^m \int_{a_j}^{b_j} A_1^j dx + \int_{a_1}^a dx \sum_{i=1}^n \int_{c_i}^{d_i} A_2^i dy - \sum_{i=1}^n \sum_{j=1}^m \int_{a_j}^{b_j} \int_{c_i}^{d_i} A_3^{ij} dxdy\right),$$
$$E_k^R = \frac{\rho}{2}\left(\int_0^b dy \sum_{j=1}^m \int_{a_j}^{b_j} A_4^j dx + \int_{a_1}^a dx \sum_{i=1}^n \int_{c_i}^{d_i} A_5^i dy - \sum_{i=1}^n \sum_{j=1}^m \int_{a_j}^{b_j} \int_{c_i}^{d_i} A_6^{ij} dxdy\right). \quad (15)$$

2.3 Dimensionless parameters

Introduction of dimensionless parameters in the calculation of shell structures makes it possible to obtain more comprehensive information about the stress-strain state of shells and to identify deformation characteristics for a series of similar shells.

When solving in dimensional parameters, the unknown functions have different order of magnitude, so the deflections W are of order 10^{-1}, and U, V, Ψ_x, Ψ_y are of order $10^{-2}-10^{-3}$. In addition, when working with small numbers, instrumental error is accumulated. When solving a problem in dimensionless parameters, the order of magnitude of unknown functions equalizes, and instrumental error accumulates less. However, the order of magnitude of load parameters $\bar{P}$ and time $\bar{t}$ can differ significantly from the order of the other parameters and be different for every specific problem. The correct selection of the accuracy parameters in the numerical solution of the ordinary differential equations (ODE) system makes it possible to fairly accurately find the values of critical loads, despite the difference in orders.

Dimensionless parameters are introduced as follows [47]:

$$\xi = \frac{x-a_1}{a-a_1}, \quad \eta = \frac{y}{b}, \quad \bar{\lambda} = \frac{aA}{bB}, \quad k_\xi = hk_x, \quad k_\eta = hk_y, \quad \bar{U} = \frac{aUA}{h^2}, \quad \bar{V} = \frac{bVB}{h^2}, \quad \bar{W} = \frac{W}{h}, \quad \bar{\Psi}_x = \frac{\Psi_x aA}{h}, \quad \bar{\Psi}_y = \frac{\Psi_y bB}{h},$$
$$\bar{t} = \frac{h}{a^2A^2}\sqrt{\frac{E}{(1-\mu^2)\rho}}\cdot t, \quad \bar{P} = \frac{a^4A^4q}{h^4E}, \quad \bar{A} = \frac{aA}{h}, \quad \bar{B} = \frac{bB}{h}, \quad \bar{z} = \frac{z}{h}. \quad (16)$$

Conversion to dimensionless parameters in the expressions E_s, E_k was discussed earlier in [47, 48], where the following was derived:

$$E_s = \frac{Eh^7}{2(1-\mu^2)a^4A^4}\bar{E}_s, \quad E_k = \frac{Eh^7}{2(1-\mu^2)a^4A^4}\bar{E}_k.$$

Despite the fact that dimensionless parameters are used in all calculations in software implementation, all results will be provided in dimensional parameters for interpretation convenience.

2.4 Numerical methods

The calculation algorithm is based on the L.V. Kantorovich methods (for reducing the system of differential equations for functions of three variables to a system of ordinary differential equations (ODE) with respect to the functions of only one variable t) and the Rosenbrock method (for the numerical solution of stiff ODE systems).

The L.V. Kantorovich method is used for reduction of the multidimensional functional to the one-dimensional one [47]. For this, the unknown functions of displacements and rotation angles of the normal are presented in the following form:

$$U(x,y,t) = \sum_{k=1}^{\sqrt{N}}\sum_{l=1}^{\sqrt{N}} U_{kl}(t) X_1^k Y_1^l, \qquad V(x,y,t) = \sum_{k=1}^{\sqrt{N}}\sum_{l=1}^{\sqrt{N}} V_{kl}(t) X_2^k Y_2^l, \qquad W(x,y,t) = \sum_{k=1}^{\sqrt{N}}\sum_{l=1}^{\sqrt{N}} W_{kl}(t) X_3^k Y_3^l,$$
$$\Psi_x(x,y,t) = \sum_{k=1}^{\sqrt{N}}\sum_{l=1}^{\sqrt{N}} \Psi_{xkl}(t) X_4^k Y_4^l, \qquad \Psi_y(x,y,t) = \sum_{k=1}^{\sqrt{N}}\sum_{l=1}^{\sqrt{N}} \Psi_{ykl}(t) X_5^k Y_5^l, \quad (17)$$

where $U_{kl}-\Psi_{ykl}$ are unknown variable functions of t; and $X_1^k,...,X_5^k$, $Y_1^l,...,Y_5^l$ are known approximation functions of the arguments x and y that satisfy the given boundary conditions.

Boundary conditions are chosen depending on the fastening method of the shell contour. When using the Timoshenko–Reissner model, five boundary conditions must be satisfied at each edge of the shell. Considering simply support thin-walled shells (at $x=0, x=a$: $U=V=W=M_x=\Psi_y=0$; at $y=0, y=b$: $U=V=W=M_y=\Psi_x=0$).

Further, functions (17) are substituted into the functional of total deformation energy of a shell (5). After calculation of the integrals on the variables x and y from the known functions, the functional I represents one-dimensional functional of the functions $U_{kl}(t)-\Psi_{ykl}(t)$. From the conditions for the minimum of this functional $\delta I = 0$, equations of motion are found which are a system of ordinary differential equations (ODE). Also, the system obtained in this manner is called a multidimensional variation of the Euler–Lagrange equation:

$$\frac{d}{dt}\frac{\partial(E_k-E_s)}{\partial \dot{X}_j(t)} - \frac{\partial(E_k-E_s)}{\partial X_j(t)} = 0, \quad j=1,2,...,5N, \quad (18)$$

where $X(t) = \left(U_{kl}(t), V_{kl}(t), W_{kl}(t), \Psi_{xkl}(t), \Psi_{ykl}(t)\right)^T$, $k,l = 1,..,\sqrt{N}$, and the dot denotes the time derivative.

Since the derivatives of the unknown functions with respect to the variable t are contained only in the expression for kinetic energy, and the functions themselves only in the expression for E_s, then the following is valid:

$$\frac{d}{dt}\frac{\partial E_k}{\partial \dot{X}_j(t)} + \frac{\partial E_s}{\partial X_j(t)} = 0, \quad j=1,2,...,5N. \quad (19)$$

Table 2. Material parameters

	E, MPa	μ	ρ, kg / m^3	σ_T, MPa
Steel S345	2.1×10^5	0.3	7800	345

Moreover, $\partial E_s / \partial X_j(t) = 0$, $j = 1, 2, ..., 5N$ is a system of equations for the static problem [46]. The system must be solved under the initial conditions at $t = 0$:

$$U_{kl} = V_{kl} = W_{kl} = \Psi_{xkl} = \Psi_{ykl} = 0, \quad \dot{U}_{kl} = \dot{V}_{kl} = \dot{W}_{kl} = \dot{\Psi}_{xkl} = \dot{\Psi}_{ykl} = 0, \quad k, l = 1, .., \sqrt{N}. \tag{20}$$

The process of formation of system (19) was programmed in the analytical computing system Maple 2019. The resulting ODE system was solved numerically using the Rosenbrock method (embedded in Maple 2019), which is effective for solving stiff systems.

3. Numerical Results

In order to demonstrate the applicability of the proposed mathematical model and algorithm, calculations of the buckling of shell structures will be performed.

Two types of structures will be considered: doubly-curved shallow shells, having a square base and cylindrical panels.

Here and further, for the convenience all results and input values are given in dimensional parameters, and moreover all the calculations in the computational software are performed in dimensionless parameters.

For further calculations, it is taken $N = 9$ (justification for this will be shown below).

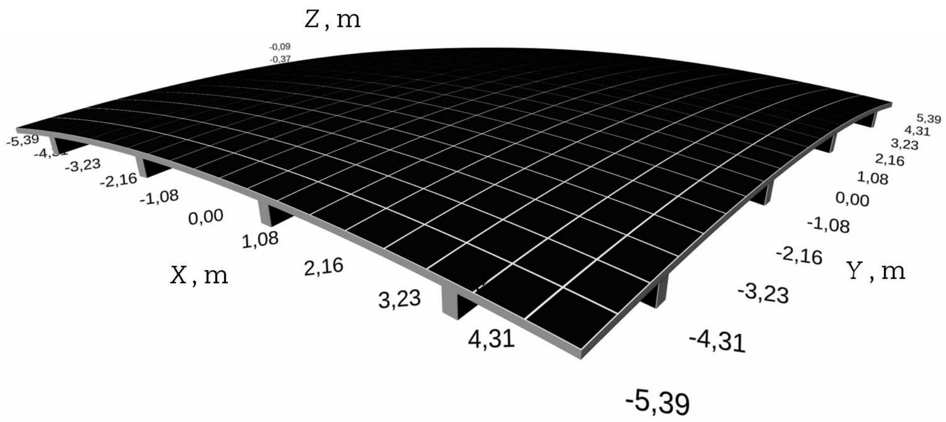

Fig. 2. The considered shallow shell of double curvature in the global Cartesian coordinate system

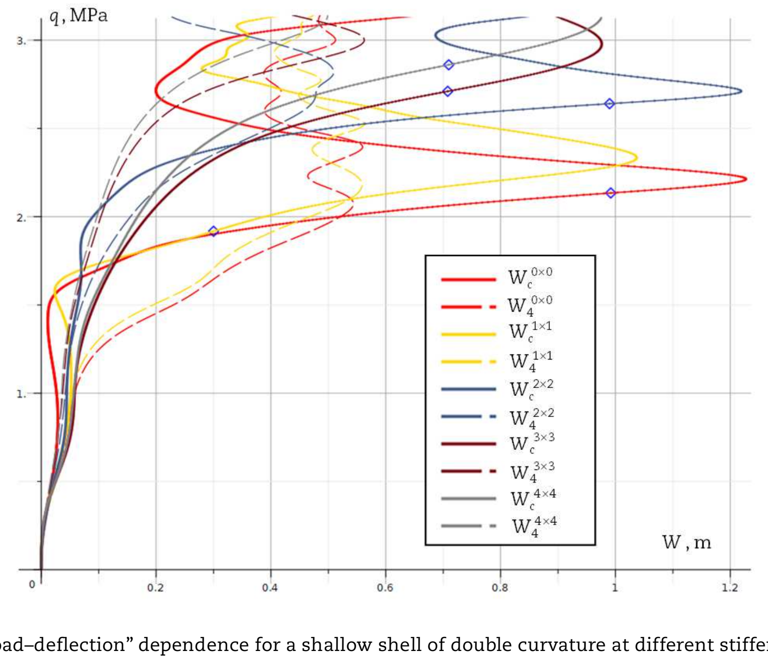

Fig. 3. The “load–deflection” dependence for a shallow shell of double curvature at different stiffeners scheme

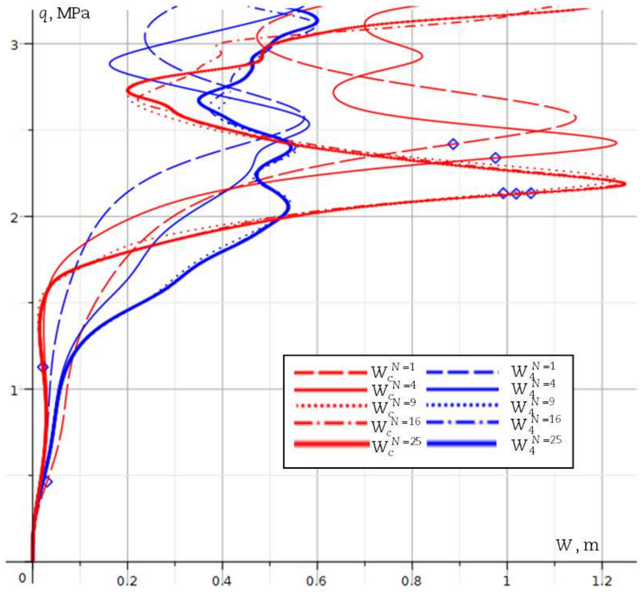

Fig. 4. The "load–deflection" dependence for a shallow shell of double curvature at different values of *N* (stiffeners scheme 0×0)

Table 3. Phase portrait for a double-curved shell with a different number of stiffeners of $A_1 = 27.2$ MPa/s

Ribs scheme	W_c	W_4
0×0	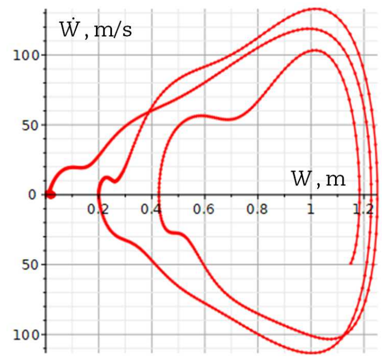	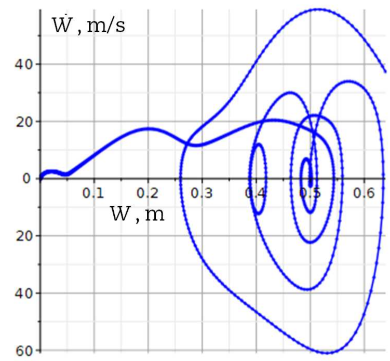
1×1	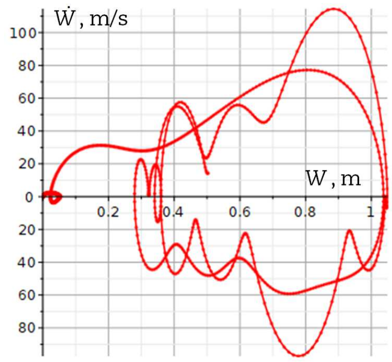	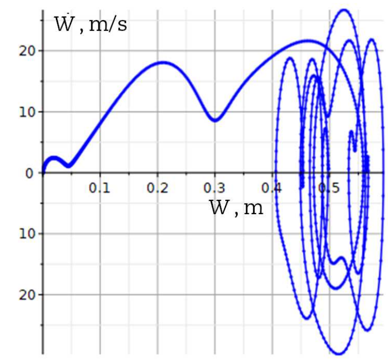
2×2	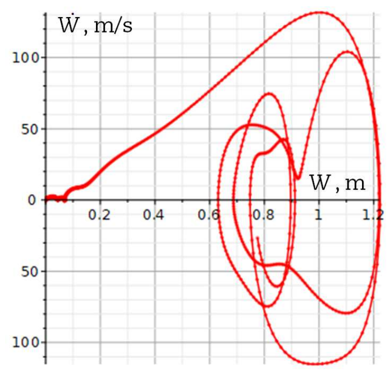	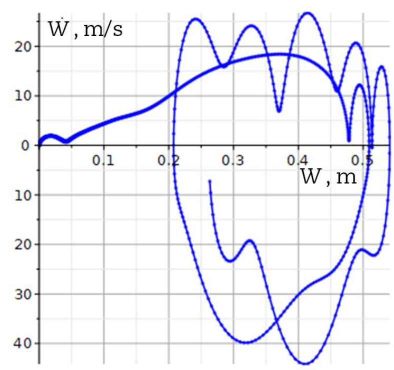

Table 3. Continued

<table>
<tr><th>Ribs scheme</th><th>W_c</th><th>W_4</th></tr>
<tr><td>3×3</td><td>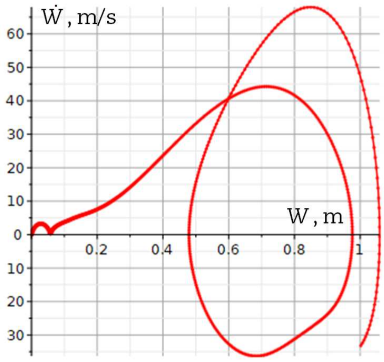
</td><td>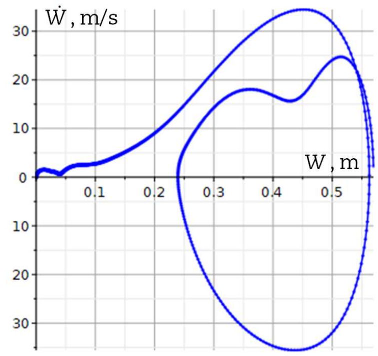
</td></tr>
<tr><td>4×4</td><td>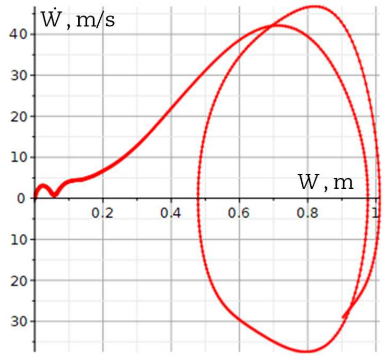
</td><td>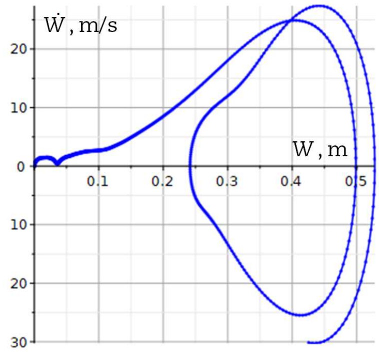
</td></tr>
</table>

3.1 Material, loading and stiffeners parameters

Mechanical characteristics of materials of the structures being studied are shown in Table 2. Structures subjected to the external uniformly distributed lateral load $q = q(x,y,t) = q_{sv} + A_1 t$, $P_x = P_x(x,y) = P_{xsv}$, $P_y = P_y(x,y) = P_{ysv}$, where q_{sv}, P_{xsv}, P_{ysv} – self-weight load.

The shells are reinforced with an orthogonal grid of stiffeners uniformly distributed throughout the structure. The width of the stiffeners is $r^j = r^i = 2h$, and the height is $h^j = h^i = 3h$. The distance between the stiffeners are defined as x_r. The outer stiffeners will be at a distance $0.5x_r$ from the edge of the structure.

3.2 Doubly-curved shallow shells

In selecting such a structure, in correlations of the mathematical model it is necessary to take $A = B = 1$, $R_1 = const$, $R_2 = const$.

Geometrical parameters: $h = 0.09$ m, $a = b = 10.8$ m, $R_1 = R_2 = 40.05$ m, $a_1 = 0$. The rate of loading of $A_1 = 27.2$ MPa/s.

In Fig. 2, the considered structure with an orthogonal grid of stiffeners 4×4 is shown in the global Cartesian coordinate system (X,Y,Z).

A comparison of "load–deflection" curves for the examined shell made of Steel S345, depending on the number of stiffeners (the upper index in the diagram notations) is shown in Figure 3. Here and further, the red curve W_c in the diagrams depicts the deflection in the center of a structure $\left(x = (a_1 + a)/2, y = b/2\right)$, and the blue curve W_4 the deflection in the quadrant of a structure $\left(x = (3a_1 + a)/4, y = b/4\right)$. In the deflection diagram, the value corresponding to buckling is marked with a blue dot in the center (corresponds to the inflection point). The results show that an increase in the number of stiffeners from 1×1 to 2×2. has the greatest impact on the increase of the critical load value.

The justification for the choice of the number of terms in (17) (value of N) is shown in Figure 4. As can be seen from the graph, the shape of the curves for the values $N = 9$, $N = 16$, $N = 25$ is practically the same.

In Table 3 the phase portrait (dependence between W and $\partial W/\partial t$) for a double-curved shell with a different number of stiffeners of $A_1 = 27.2$ MPa/s are shown.

It is also common for this type of structure to have the highest deflection in the center with significantly greater amplitude than in a quarter. Analysis of different points of the structure, such as the center or quarter, allows to evaluate the processes of formation, distribution and redistribution of local dents. Also, it is often difficult to fully assess the process of deformation of a structure from one curve, since a significant increase in dents can occur only in a separate part of it.

When evaluating vibration processes, based on these data, it is possible to identify the vibration of separate parts of the structure in antiphase, which can lead to peak stress values.

In Table 4 critical buckling loads q_{cr} for doubly-curved shell via different methods and stiffening scheme are shown. In addition to the discrete refined method, proposed by the author, the previously used method is presented (curves $\tilde{W}$ on Fig. 5), without taking into account the refinement coefficients (11). It should be noted that the complex nature of the load/deflection curves makes the unambiguous determination of critical load values a lot harder.

In the Fig. 5 the "load–deflection" dependence for a shallow shell of double curvature with different methods of taking into account stiffeners are presented for stiffening scheme 1×1 and 4×4. As follows from the foregoing, the critical load values derived when using the common discrete method can be significantly overestimated. With the usual discrete method, the coefficients (11) are not taken into account (i.e., in fact, their value is equal to 1). If the coefficients (11) are taken into account, then their values are less than 1, therefore, the real rigidity of the structure is less than that obtained with the common discrete method, and, consequently, the value of the critical load is also less. With an increase in the number of stiffeners, this discrepancy accumulates.

Table 4. Critical buckling loads for doubly-curved shell via different methods and stiffening scheme

Method	Critical buckling load q_{cr}, MPa				
	0×0	1×1	2×2	3×3	4×4
Discrete	2.1328	2.5265	2.7448	3.0829	3.2685
Refined discrete (Semenov)	2.1328	1.9172	2.6401	2.7102	2.8605

3.3 Panels of cylindrical shells

Panels of cylindrical shells are studied (Fig. 1b). In selecting such a structure, in correlations of the mathematical model it is necessary to take $A=1$, $B=R_2$, $R_1=\infty$, $R_2=const$.

Geometrical parameters: $h=0.08$ m, $a=16$ m, $b=1$ rad, $R_2=16$ m, $a_1=0$.

The rate of loading of $A_1=10$ MPa/s.

In Fig. 6 the considered structure with an orthogonal grid of stiffeners 8×8 is shown in the global Cartesian coordinate system (X,Y,Z).

A comparison of “load–deflection” curves for the examined shell made of Steel S345, depending on the number of stiffeners (the upper index in the diagram notations) is shown in Figure 7. It should be noted that in the given structure local buckling is observed prior to the general buckling.

In Table 5 the phase portrait (dependence between W and $\partial W/\partial t$) for a cylindrical shell panel with a different number of stiffeners of $A_1=10$ MPa/s are shown.

For this structure, it is of interest to change the nature of the deformation of the points of the center and the quarter with an increase in the number of stiffeners (more than 2×2). The central point began to bulge upward, and the quarter point began to bulge downward. Also, with an increase of the number of ribs, the maximum values of deflections significantly decreased, which indicates their effectiveness.

It can be seen from the phase portraits that with an increase in the number of stiffeners, the maximum deflection change rates at the central point decrease and become close in values to the maximum rates in the quarter. Thus, with an increase in the number of stiffeners, the vibration process in different parts of the structure is leveled out, and the deformation of the structure occurs more stably.

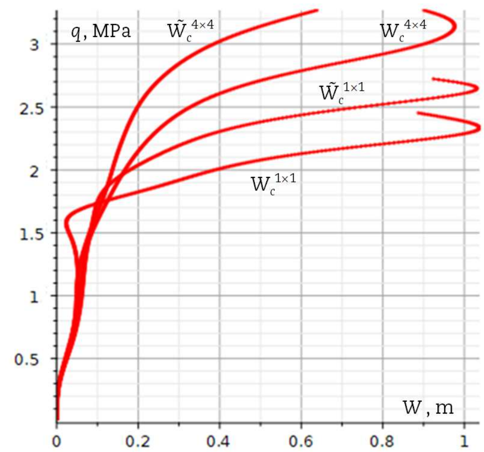

Fig. 5. The “load–deflection” dependence for a shallow shell of double curvature with different methods of taking into account stiffeners

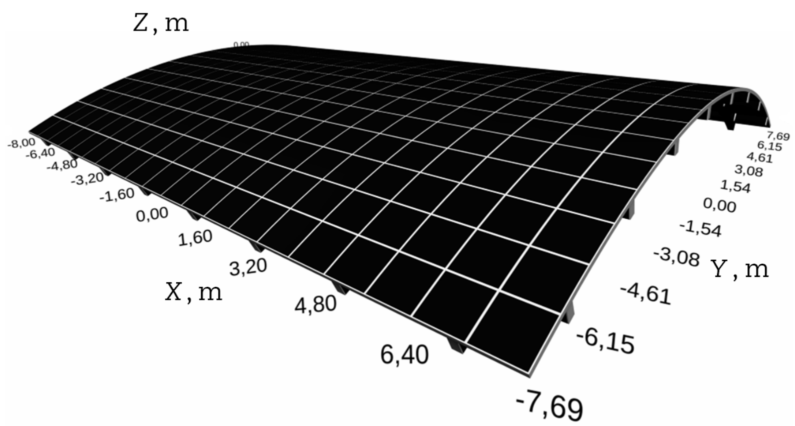

Fig. 6. The considered cylindrical panel in the global Cartesian coordinate system

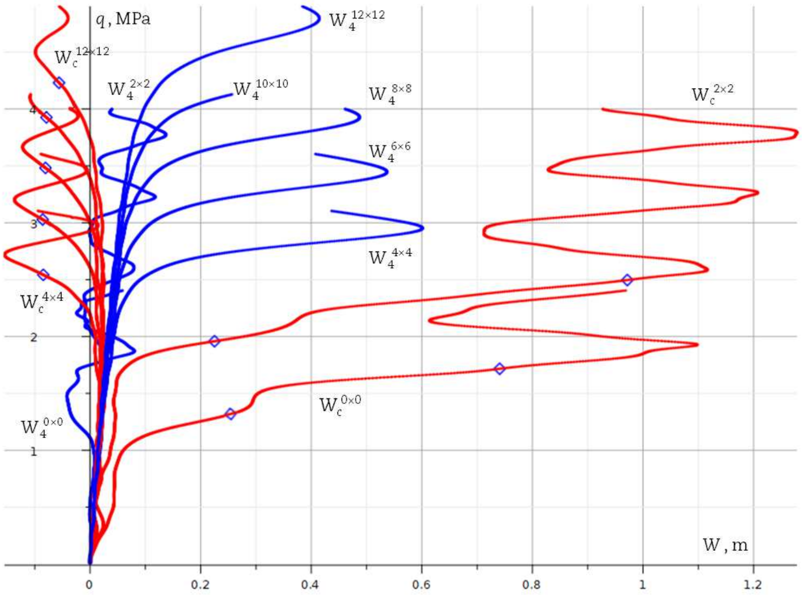

Fig. 7. The "load–deflection" dependence for the cylindrical panel being studied at different values of the rate of loading

Table 5. Phase portrait for a cylindrical shell panel with a different number of stiffeners of $A_1 = 10$ MPa/s

Ribs scheme	W_c	W_4
0×0	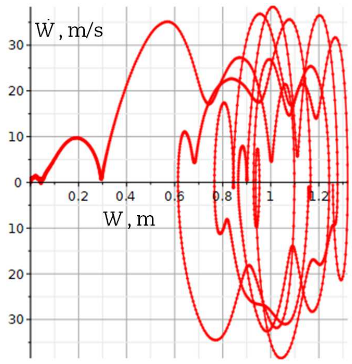	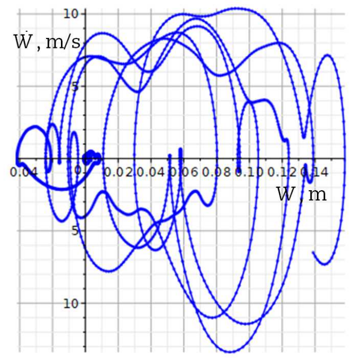
2×2	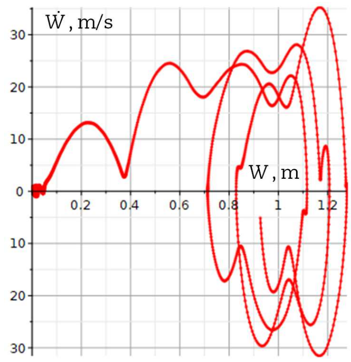	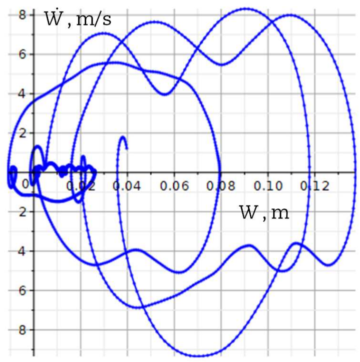
4×4	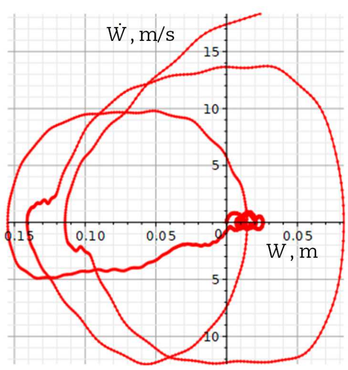	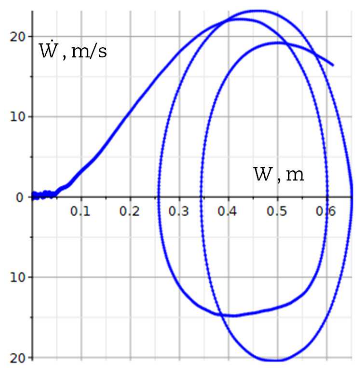

Table 5. Continued

Ribs scheme	W_c	W_4
6 × 6	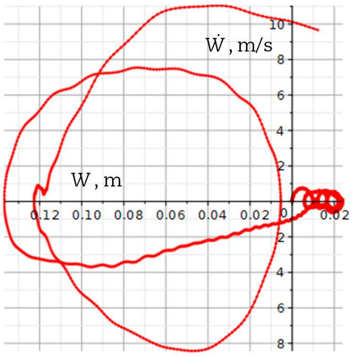	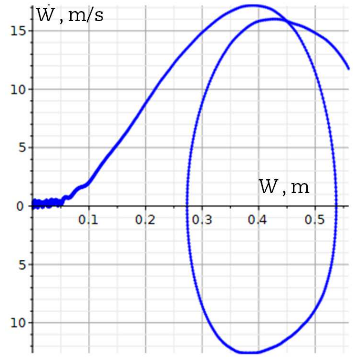
8 × 8	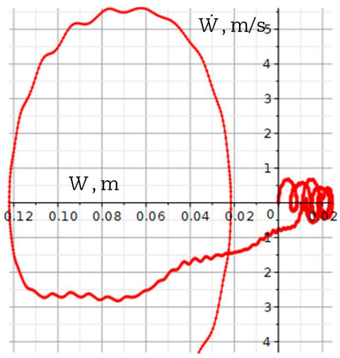	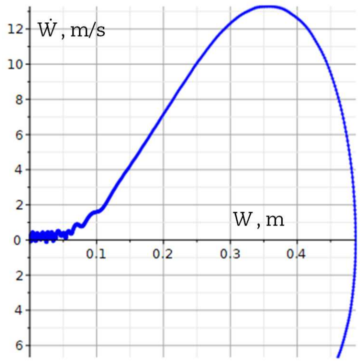
10 × 10	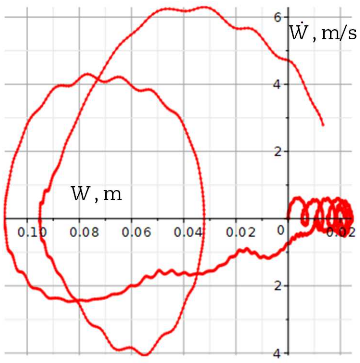	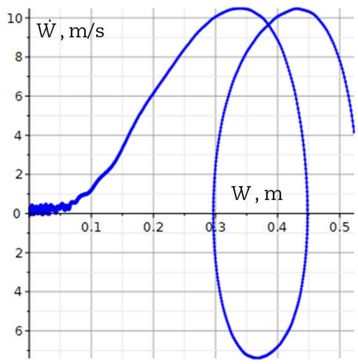
12 × 12	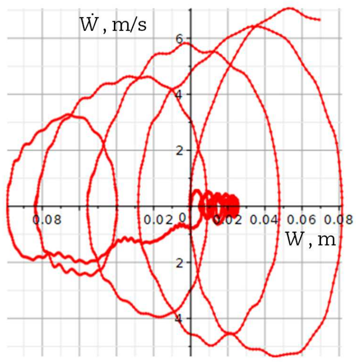	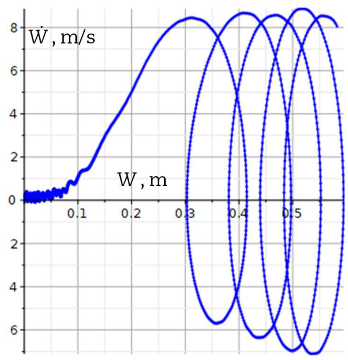

4. Discussion on the Results and Conclusions

Therefore, this paper presents a new mathematical model of shell structure deformation under dynamic loading, taking into account geometrical nonlinearity, transverse shears, and stiffeners. A distinctive feature of the model is the use of the refined discrete method to account for stiffeners, suggested by the author earlier in [45]. The method has previously been used only in static problems [46].

It uses adjusting normalizing factors and makes it possible to obtain the most correct critical load values. A comparison with the common discrete method shows a decrease in the critical load (refined discrete method), which may be essential when assessing the operation capability of a structure.

Data on the deformation of shells under consideration (shallow doubly curved shells and cylindrical panels) were obtained for the case of reinforcement with an orthogonal grid of stiffeners. Buckling load values were derived. The calculations showed the effectiveness of such reinforcement and can serve as a basis for further research on other reinforcement options.

The position of the stiffeners can certainly affect the dynamic buckling behaviors of the shell. Thus, it is essential conduct optimization analysis about the stiffener positions and numbers, and this issue can be the subject of further research. For such an analysis, for example, multi-dimensional global optimization algorithms can be applied, described in [49].

For all problems under consideration, phase portraits of the system were given, which can be used to analyze the process of system deformation.

Through the example of one of the problems, it was demonstrated that the Kantorovich method converges with an increase in the number of summands in the expansion of the unknown functions in series.

Author Contributions

Not Applicable.

Acknowledgments

The author would like to thank Yu.N. Zgoda for his help in preparing Figures 2 and 6.

Conflict of Interest

The author declared no potential conflicts of interest with respect to the research, authorship, and publication of this article.

Funding

The author received no financial support for the research, authorship, and publication of this article.

Data Availability Statements

Not Applicable.

Nomenclature

A, B	Lame parameters describing the shell geometry;	$N_x^R, N_y^R, N_{xy}^R, N_{yx}^R$	Forces and moments, occurring in the stiffeners;
A_1	Rate of loading;	N	Number of terms in the expansion of Ritz method;
E	Elastic modulus;	q, P_x, P_y	Load components;
E_s	Functional of potential deformation energy of the shell structure;	q_{cr}	Critical buckling load;
E_s^0	Functional of potential deformation energy of the skin;	Q_x, Q_y	Transverse forces in the planes *xOz* and *yOz*;
E_p^R	Potential deformation energy of the stiffeners;	r^j, r^i	Width of the stiffeners;
E_k	Kinetic deformation energy of the shell structure;	x_r	Distance between the stiffeners;
E_k^0	Kinetic deformation energy of the skin;	U, V, W	Displacement functions;
E_k^R	Kinetic deformation energy of the stiffeners;	W_c	Deflection in the center of a structure;
$f(z)$	Function describing the distribution of stresses τ_{xz} and τ_{yz} through the shell thickness;	W_4	Deflection in the quadrant of a structure;
G_{12}, G_{13}, G_{23}	Shear modules;	γ_{xy}	Shear deformation in the *xOy* plane;
h	Thickness of the skin;	$\chi_1, \chi_2, \chi_{12}$	Functions of curvature and torsional change;
h^i, h^j	Height of stiffeners;	Ψ_x, Ψ_y	Functions of the normal rotation angles in the *xOz* and *yOz* planes, respectively;
k_x, k_y	Main curvatures of the shell along the *x* and y axes;	$\varepsilon_x, \varepsilon_y$	Deformations of elongation along the *x*, *y* coordinates of the middle surface;
n, m	Number of stiffeners;	μ	Poisson's ratio;
M_x, M_y, M_{xy}, M_{yx}	Moments, occurring in the structure;	ρ	Density of the material;
$M_x^0, M_y^0, M_{xy}^0, M_{yx}^0$	Moments, occurring in the skin;	σ_x, σ_y	The normal stresses in the directions of axes x, y;
$M_x^R, M_y^R, M_{xy}^R, M_{yx}^R$	Forces and moments, occurring in the stiffeners;	$\tau_{xy}, \tau_{xz}, \tau_{yz}$	Shear stresses in the plane *xOy*, *xOz* and *yOz*;
N_x, N_y, N_{xy}, N_{yx}	Forces, occurring in the structure;	σ_i	Stress intensity;
$N_x^0, N_y^0, N_{xy}^0, N_{yx}^0$	Forces, occurring in the skin;	σ_T	Material yield strength.

References

[1] Sowiński, K., The Ritz method application for stress and deformation analyses of standard orthotropic pressure vessels, *Thin-Walled Structures*, 162, 2021, 107585. DOI: 10.1016/j.tws.2021.107585.

[2] Radchenko, P.A., Batuev, S.P., Radchenko, A.V., Plevkov, V.S., Numerical modeling of the destruction of a shell made of concrete and fiber-reinforced concrete under impulse action, *Omsk Scientific Bulletin*, 3(143), 2015, 345–348. (in Russian)

[3] Raeesi, A., Ghaednia, H., Zohrehheydariha, J., Das, S., Failure analysis of steel silos subject to wind load, *Engineering Failure Analysis*, 79, 2017, 749–761. DOI: 10.1016/j.engfailanal.2017.04.031.
[4] Amabili, M., Non-linearities in rotation and thickness deformation in a new third-order thickness deformation theory for static and dynamic analysis of isotropic and laminated doubly curved shells, *International Journal of Non-Linear Mechanics*, 69, 2015, 109–128. DOI: 10.1016/j.ijnonlinmec.2014.11.026.
[5] Xie, K., Chen, M., Zhang, L., Xie, D., Free and forced vibration analysis of non-uniformly supported cylindrical shells through wave based method, *International Journal of Mechanical Sciences*, 128–129, 2017, 512–526. DOI: 10.1016/j.ijmecsci.2017.05.014.
[6] Dey, T., Ramachandra, L.S., Static and dynamic instability analysis of composite cylindrical shell panels subjected to partial edge loading, *International Journal of Non-Linear Mechanics*, 64, 2014, 46–56. DOI: 10.1016/j.ijnonlinmec.2014.03.014.
[7] Hao, Y.X., Li, Z.N., Zhang, W., Li, S.B., Yao, M.H., Vibration of functionally graded sandwich doubly curved shells using improved shear deformation theory, *Science China Technological Sciences*, 61(6), 2018, 791–808. DOI: 10.1007/s11431-016-9097-7.
[8] Krysko, A.V., Awrejcewicz, J., Saltykova, O.A., Vetsel, S.S., Krysko, V.A., Nonlinear dynamics and contact interactions of the structures composed of beam-beam and beam-closed cylindrical shell members, *Chaos, Solitons & Fractals*, 91, 2016, 622–638. DOI: 10.1016/j.chaos.2016.09.001.
[9] Gonçalves, P.B., Silva, F.M.A., Del Prado, Z.J.G.N., Reduced Order Models for the Nonlinear Dynamic Analysis of Shells, *Procedia IUTAM*, 19, 2016, 118–125. DOI: 10.1016/j.piutam.2016.03.016.
[10] Leonenko, D.V., Starovoitov, E.I., Vibrations of Cylindrical Sandwich Shells with Elastic Core under Local Loads, *International Applied Mechanics*, 52(4), 2016, 359–367. DOI: 10.1007/s10778-016-0760-8.
[11] Lee, Y.-S., Kim, Y.-W., Effect of boundary conditions on natural frequencies for rotating composite cylindrical shells with orthogonal stiffeners, *Advances in Engineering Software*, 30(9-11), 1999, 649–655. DOI: 10.1016/S0965-9978(98)00115-X.
[12] Mustafa, B.A.J., Ali, R., An energy method for free vibration analysis of stiffened circular cylindrical shells, *Computers & Structures*, 32(2), 1989, 355–363. DOI: 10.1016/0045-7949(89)90047-3.
[13] Talebitooti, M., Ghayour, M., Ziaei-Rad, S., Talebitooti, R., Free vibrations of rotating composite conical shells with stringer and ring stiffeners, *Archive of Applied Mechanics*, 80(3), 2010, 201–215. DOI: 10.1007/s00419-009-0311-4.
[14] Wang, C.M., Swaddiwudhipong, S., Tian, J., Ritz Method for Vibration Analysis of Cylindrical Shells with Ring Stiffeners, *Journal of Engineering Mechanics*, 123(2), 1997, 134–142. DOI: 10.1061/(ASCE)0733-9399(1997)123:2(134).
[15] Qu, Y., Wu, S., Chen, Y., Hua, H., Vibration analysis of ring-stiffened conical-cylindrical-spherical shells based on a modified variational approach, *International Journal of Mechanical Sciences*, 69, 2013, 72–84. DOI: 10.1016/j.ijmecsci.2013.01.026.
[16] Zhao, X., Liew, K.M., Ng, T.Y., Vibrations of rotating cross-ply laminated circular cylindrical shells with stringer and ring stiffeners, *International Journal of Solids and Structures*, 39(2), 2002, 529–545. DOI: 10.1016/S0020-7683(01)00194-9.
[17] Jafari, A.A., Bagheri, M., Free vibration of non-uniformly ring stiffened cylindrical shells using analytical, experimental and numerical methods, *Thin-Walled Structures*, 44(1), 2006, 82–90. DOI: 10.1016/j.tws.2005.08.008.
[18] Khalmuradov, R.I., Ismoilov, E.A., Nonlinear vibrations of a circular plate reinforced by ribs, *IOP Conf. Ser.: Earth Environ. Sci.*, 614, 2020, 012071. DOI: 10.1088/1755-1315/614/1/012071.
[19] Peng-Cheng, S., Dade, H., Zongmu, W., Static, vibration and stability analysis of stiffened plates using B spline functions, *Computers & Structures*, 27(1), 1987, 73–78. DOI: 10.1016/0045-7949(87)90182-9.
[20] Dung, D.V., Nam, V.H., An analytical approach to analyze nonlinear dynamic response of eccentrically stiffened functionally graded circular cylindrical shells subjected to time dependent axial compression and external pressure. Part 2: Numerical results and discussion, *Vietnam Journal of Mechanics*, 36(4), 2014, 255–265. DOI: 10.15625/0866-7136/36/4/3986.
[21] Azarboni, H.R., Ansari, R., Nazarinezhad, A., Chaotic dynamics and stability of functionally graded material doubly curved shallow shells, *Chaos, Solitons & Fractals*, 109, 2018, 14–25. DOI: 10.1016/j.chaos.2018.02.011.
[22] Bich, D.H., Long, V.D., Non-linear dynamical analysis of imperfect functionally graded material shallow shells, *Vietnam Journal of Mechanics*, 32(1), 2010, 1–14. DOI: 10.15625/0866-7136/32/1/312.
[23] del Prado, Z., Gonçalves, P.B., Païdoussis, M.P., Non-linear vibrations and instabilities of orthotropic cylindrical shells with internal flowing fluid, *International Journal of Mechanical Sciences*, 52(11), 2010, 1437–1457. DOI: 10.1016/j.ijmecsci.2010.03.016.
[24] Jansen, E.L., Dynamic Stability Problems of Anisotropic Cylindrical Shells via a Simplified Analysis, *Nonlinear Dynamics*, 39(4), 2005, 349–367. DOI: 10.1007/s11071-005-4343-1.
[25] Chamis, C.C., Dynamic Buckling and Postbuckling of a Composite Shell, *International Journal of Structural Stability and Dynamics*, 10(4), 2010, 791–805. DOI: 10.1142/S0219455410003749.
[26] Kubenko, V.D., Koval'chuk, P.S., Nonlinear problems of the dynamics of elastic shells partially filled with a liquid, *International Applied Mechanics*, 36(4), 2000, 421–448. DOI: 10.1007/BF02681969.
[27] Xin, J., Wang, J., Yao, J., Han, Q., Vibration, Buckling and Dynamic Stability of a Cracked Cylindrical Shell with Time-Varying Rotating Speed, *Mechanics Based Design of Structures and Machines*, 39(4), 2011, 461–490. DOI: 10.1080/15397734.2011.569301.
[28] Gao, K., Gao, W., Wu, D., Song, C., Nonlinear dynamic stability of the orthotropic functionally graded cylindrical shell surrounded by Winkler-Pasternak elastic foundation subjected to a linearly increasing load, *Journal of Sound and Vibration*, 415, 2018, 147–168. DOI: 10.1016/j.jsv.2017.11.038.
[29] Lavrenčič, M., Brank, B., Simulation of shell buckling by implicit dynamics and numerically dissipative schemes, *Thin-Walled Structures*, 132, 2018, 682–699. DOI: 10.1016/j.tws.2018.08.010.
[30] Li, Z.-M., Liu, T., Qiao, P., Nonlinear vibration and dynamic instability analyses of laminated doubly curved panels in thermal environments, *Composite Structures*, 267, 2021, 113434. DOI: 10.1016/j.compstruct.2020.113434.
[31] Zhou, Y., Stanciulescu, I., Eason, T., Spottswood, M., Fast approximations of dynamic stability boundaries of slender curved structures, *International Journal of Non-Linear Mechanics*, 95, 2017, 47–58. DOI: 10.1016/j.ijnonlinmec.2017.06.002.
[32] Ren, S., Song, Y., Zhang, A.-M., Wang, S., Li, P., Experimental study on dynamic buckling of submerged grid-stiffened cylindrical shells under intermediate-velocity impact, *Applied Ocean Research*, 74, 2018, 237–245. DOI: 10.1016/j.apor.2018.02.018.
[33] Patel, S.N., Datta, P.K., Sheikh, A.H., Buckling and dynamic instability analysis of stiffened shell panels, *Thin-Walled Structures*, 44(3), 2006, 321–333. DOI: 10.1016/j.tws.2006.03.004.
[34] Amiro, I.Ya., Zarutskii, V.A., Stability of ribbed shells, *Soviet Applied Mechanics*, 19(11), 1983, 925–940. DOI: 10.1007/BF01362647.
[35] Sadeghifar, M., Bagheri, M., Jafari, A.A., Buckling analysis of stringer-stiffened laminated cylindrical shells with nonuniform eccentricity, *Archive of Applied Mechanics*, 81(7), 2011, 875–886. DOI: 10.1007/s00419-010-0457-0.
[36] Huang, S., Qiao, P., A new semi-analytical method for nonlinear stability analysis of stiffened laminated composite doubly-curved shallow shells, *Composite Structures*, 251, 2020, 112526. DOI: 10.1016/j.compstruct.2020.112526.
[37] Ghasemi, A.R., Tabatabaeian, A., Hajmohammad, M.H., Tornabene, F., Multi-step buckling optimization analysis of stiffened and unstiffened polymer matrix composite shells: A new experimentally validated method, *Composite Structures*, 273, 2021, 114280. DOI: 10.1016/j.compstruct.2021.114280.
[38] Dai, Q., Cao, Q., Parametric instability analysis of truncated conical shells using the Haar wavelet method, *Mechanical Systems and Signal Processing*, 105, 2018, 200–213. DOI: 10.1016/j.ymssp.2017.12.004.
[39] Polat, C., Calayir, Y., Nonlinear static and dynamic analysis of shells of revolution, *Mechanics Research Communications*, 37(2), 2010, 205–209. DOI: 10.1016/j.mechrescom.2009.12.009.
[40] Storozhuk, E.A., Yatsura, A.V., Analytical-Numerical Solution of Static Problems for Noncircular Cylindrical Shells of Variable Thickness, *International Applied Mechanics*, 53(3), 2017, 313–325. DOI: 10.1007/s10778-017-0813-7.
[41] Karpov, V., Variational method for derivation of equations of mixed type for shells of a general type, *Architecture and Engineering*, 1(2), 2016, 43–48. DOI: 10.23968/2500-0055-2016-1-2-43-48.
[42] Abrosimov, N.A., Novosel'tseva, N.A., Computer Modeling of the Dynamic Strength of Metal-Plastic Cylindrical Shells Under Explosive Loading, *Mechanics of Composite Materials*, 53(2), 2017, 139–148. DOI: 10.1007/s11029-017-9648-x.
[43] Hao, P., Liu, D., Zhang, K., Yuan, Y., Wang, B., Li, G., Zhang, X., Intelligent layout design of curvilinearly stiffened panels via deep learning-based method, *Materials & Design*, 197, 2021, 109180. DOI: 10.1016/j.matdes.2020.109180.
[44] Hao, P., Yuan, X., Liu, C., Wang, B., Liu, H., Li, G., Niu, F., An integrated framework of exact modeling, isogeometric analysis and optimization for variable-stiffness composite panels, *Computer Methods in Applied Mechanics and Engineering*, 339, 2018, 205–238. DOI: 10.1016/j.cma.2018.04.046.

[45] Karpov, V.V., Semenov, A.A., Refined model of stiffened shells, *International Journal of Solids and Structures*, 199, 2020, 43–56. DOI: 10.1016/j.ijsolstr.2020.03.019.
[46] Semenov, A., Buckling of Shell Panels Made of Fiberglass and Reinforced with an Orthogonal Grid of Stiffeners, *Journal of Applied and Computational Mechanics*, 7(3), 2021, 1856–1861. DOI: 10.22055/jacm.2021.37768.3078.
[47] Semenov, A., Mathematical model of deformation of orthotropic shell structures under dynamic loading with transverse shears, *Computers & Structures*, 221, 2019, 65–73. DOI: 10.1016/j.compstruc.2019.05.017.
[48] Semenov, A.A., Models of Deformation of Stiffened Orthotropic Shells under Dynamic Loading, *Journal of Siberian Federal University, Mathematics & Physics*, 9(4), 2016, 485–497. DOI: 10.17516/1997-1397-2016-9-4-485-497.
[49] Li, P., Wang, H., A novel strategy for the crossarm length optimization of PSSCs based on multi-dimensional global optimization algorithms, *Engineering Structures*, 238, 2021, 112238. DOI: 10.1016/j.engstruct.2021.112238.

ORCID iD

Alexey Semenov https://orcid.org/0000-0001-9490-7364

How to cite this article: Semenov A. Dynamic Buckling of Stiffened Shell Structures with Transverse Shears under Linearly Increasing Load, *J. Appl. Comput. Mech.*, 8(4), 2022, 1343–1357. https://doi.org/10.22055/jacm.2022.39718.3452